PNAS RESEARCH ARTICLE | ENGINEERING

Analytical modeling for suction cup designs for skin-interfaced wearable devices

Shupeng Li[a], John A. Rogers[b,c,d,e,f], and Yonggang Huang[a,b,c,d,1]

Affiliations are included on p. 6.

Contributed by Yonggang Huang; received April 24, 2026; accepted June 4, 2026; reviewed by Dae-Hyeong Kim, Nanshu Lu, and Matt Pharr

Stable mounting is a central requirement for skin-interfaced wearable biomedical devices, because accurate and long-term measurements with clinical utility typically demand intimate contact with the skin, whereas practical use also requires gentle removal to minimize skin irritation and damage. Existing mounting strategies often struggle to satisfy these competing requirements simultaneously, especially under prolonged wear or in the presence of sweat and moisture. Suction-based mounting has recently emerged as a promising alternative because it can provide strong, reversible, and adhesive-free attachment, yet its underlying mechanics remain insufficiently understood. Here, we establish analytical models for the deformation and force of suction cups in a fully explicit form, covering both the cone suction cup and an optimized ring suction cup design. Unlike previous approaches that rely on indirect quantities such as the pressure difference and contact radius, which are not available before experiments and therefore cannot serve as controllable design variables, the present framework yields direct relations between suction performance and geometry parameters, material properties, and loading conditions, including the maximum push down displacement and the subsequent pull up displacement. The resulting formulas agree closely with accurate numerical solutions and lead to compact scaling laws that clearly identify how geometry and material parameters govern suction performance. These results provide a quantitative and physically transparent foundation for the design of suction-based mounting strategies in wearable devices.

wearable devices | mounting strategy | suction cup | pull up force | analytical model

Significance

Medical-grade wearable devices require mounting strategies that ensure stable skin contact for accurate, long-term measurements while allowing gentle removal to avoid skin damage. Suction-based mounting is an attractive adhesive-free approach, but its mechanics have remained unclear. This work establishes fully explicit analytical models for both cone and ring-shaped suction cups, yielding direct relations among deformation, force, geometry, and material properties. The resulting scaling laws reveal the governing design principles of suction attachment and provide a quantitative framework for optimizing suction-based interfaces in wearable biomedical devices.

Wearable biomedical devices are increasingly important as integrated platforms for continuous monitoring and point-of-care diagnostics, enabled by compact form factors, soft mechanics, and wireless operation (1, 2). Physiological sensing is the most representative application, including conventional biophysical and biomechanical readouts (such as temperature, photoplethysmography, electrocardiography, and body motions) (3, 4), sweat biochemistry (5, 6), cardiovascular monitoring such as blood pressure (7, 8) and tissue characterization (9–11) etc. Across these diverse use cases, reliable device performance depends critically on a stable mounting strategy. The interface must maintain intimate and conformal contact with the skin to support accurate and long-term measurements, while also allowing gentle removal to minimize irritation or damage, particularly for neonatal and pediatric populations, whose skin is more vulnerable (12, 13).

Existing mounting strategies for skin-mounted devices can be organized into two broad classes: adhesive interfaces and mechanically fixed, adhesive-free interfaces as shown in Fig. 1. (14). Adhesive approaches rely on chemical adhesion, providing robust fixation across a wide range of users, but prolonged wear may compromise the skin barrier, and adhesive performance can degrade in hot, humid, or sweating conditions (15). Our previous work (16) introduced a thermal switchable adhesive by reducing the adhesion for harmless removal, but it is only for single-time use. Adhesive-free approaches instead use mechanical means to secure the device, including elastic bands (8), textile meshes (17), and suction-based fixtures (18, 19). Elastic bands are widely used because they are simple and broadly compatible with many body locations, but the sustained compression required for intimate coupling can alter local cutaneous perfusion and microcirculatory activity (20). On the other hand, textile- or mesh-assisted mounting offers excellent breathability, comfort, and suitability for long-term wear, but its performance depends strongly on garment fit and contact pressure, which can lead to variable skin coupling and increased motion artifacts (21).

Among these options, suction-based mounting strategies are particularly attractive because they offer simple construction, strong attachment, harmless removal, and repeatable application without chemical adhesives (18). In our recent work (22), we introduced

Author contributions: S.L., J.A.R., and Y.H. designed research; S.L. and Y.H. performed research; S.L. analyzed data; and S.L. and Y.H. wrote the paper.

Reviewers: D.-H.K., Seoul National University; N.L., University of Texas at Austin; and M.P., Texas A&M University.

Competing interest statement: Co-author J.R. appeared on several editorials/road map publications with reviewers D.H.K and N.L within the last four years.

Copyright © 2026 the Author(s). Published by PNAS. This article is distributed under Creative Commons Attribution-NonCommercial-NoDerivatives License 4.0 (CC BY-NC-ND).

[1]To whom correspondence may be addressed. Email: y-huang@northwestern.edu.

This article contains supporting information online at https://www.pnas.org/lookup/suppl/doi:10.1073/pnas.2614670123/-/DCSupplemental.

Published July 2, 2026.

Downloaded from https://www.pnas.org by NORTHWESTERN UNIVERSITY; SERIALS DEPARTMENT on July 2, 2026 from IP address 165.124.167.3.

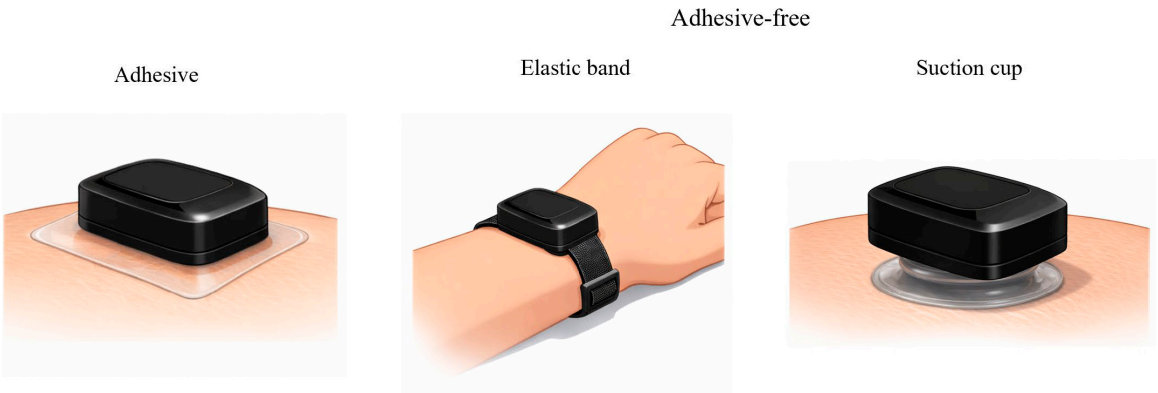

Fig. 1. Schematic illustration of different mounting methods, including adhesive interfaces and adhesive-free interfaces (with elastic band or suction cup).

this concept on a skin-interfaced platform that secures a sealed chamber to the skin for monitoring epidermal molecular flux. This mode of attachment may be especially advantageous in moist environments, including sweating or water exposure, where liquid at the interface can help suppress air leakage and preserve sealing. Although this suction cup approach has been widely used and accepted in daily life, as far as we know, current studies are mostly limited to experimental or numerical studies (18, 23–28) with no detailed analytical modeling on its mechanics deformation. The empirical equation $F = \Delta P \times \pi R_c^2$ is still widely used to estimate the detachment force of suction cups, where the pressure difference ΔP between the inside and outside suction cup and the contact radius R_c (Fig. 2*B*) are indirect variables, i.e., they are unknown before measured in experiments, thereby cannot be controlled/optimized in terms of the geometry and material properties.

In this paper, we establish a mechanics framework for suction-based skin mounting and derive analytical solutions for the deformation and pull up forces of suction cups. A cone suction cup is first analyzed as a simple baseline geometry to illustrate the analytical procedure and the form of the solution. Building on this foundation, we then develop the model for an optimized ring suction cup, which represents the primary design of interest for practical wearable devices (22) because its geometry can substantially enhance the pull up force. A modified ideal gas law is used during pull up. The analytical solutions clearly show the dependence of each geometry and material parameters, providing quantitative design guidelines for suction-based mounting strategies in wearable devices.

Results and Discussion

Cone Suction Cup. The schematic diagram in Fig. 2*A* shows the basic axisymmetric geometry (cone shape) of a cone suction cup placed on a rigid flat surface. Its axisymmetric cross-section (Fig. 2*B*) has radius R and angle θ. The suction cup has frictionless and nonadhesive surface contact after a relatively large push down displacement w_0 at its top, and its contact radius R_c is to be determined (Fig. 2*B*).

The suction cup is modeled as elastic thin plate and the Kirchhoff–Love plate theory (29) is used to relate the axisymmetric deflection w of the suction cup to the pressure p,

$$D\nabla^4 w = p, \qquad [1]$$

where the plate bending stiffness $D = \frac{Eh^3}{12(1-\nu^2)}$ is related to the Young's modulus E, Poisson's ratio ν, and plate thickness h. The present analytical model neglects transverse shear deformation, membrane stretching, shell-curvature effects, material nonlinearity at large strain, and possible local instabilities such as wrinkling or buckling. This approximation is validated by the finite element analysis (FEA) in *SI Appendix*, *Supplementary Note 5*.

For the contact region (R_c, R), the deflection is simply $w = (R-r)\tan\theta$, i.e., the vertical distance from the suction cup to the rigid flat surface at its bottom. This yields a vanishing second-order derivative $w'' = 0$ in the entire contact region.

For the noncontact region $(0, R_c)$, the pressure p is zero. The boundary conditions for Eq. **1** in the polar coordinate r are $w(0) = w_0$ and zero slope $w'(0) = 0$ at the center, and continuity of deflection $w(R_c) = (R-R_c)\tan\theta$ and slope $w'(R_c) = -\tan\theta$ at the boundary (i.e., the interface with the contact region). The deflection is then completely solved as (*SI Appendix*, *Supplementary Note 1*)

$$w_{push\ down} = w_0 - \tan\theta\frac{r^2}{R_c}\ln\frac{r}{R_c} + \left[w_0 - (R-R_c)\tan\theta\right]\frac{r^2}{R_c^2}\left(2\ln\frac{r}{R_c} - 1\right). \qquad [2]$$

Continuity of bending moment $M_r = -D\left(w'' + \nu\frac{1}{r}w'\right)$ (29) across the interface $r = R_c$ then gives $w''(R_c) = 0$, which yields the contact radius R_c during push down

$$\frac{w_0}{\tan\theta} = R - \frac{R_c}{4}. \qquad [3]$$

i.e., R_c decreases as the deflection w_0 increases, and the range of w_0 for surface contact should be $\left[\frac{3}{4}R\tan\theta, R\tan\theta\right]$. Fig. 2*C* illustrates the normalized profiles ($z^* = \frac{(R-r)\tan\theta - w}{R\tan\theta}$ vs. $r^* = \frac{r}{R}$) during push down of the suction cup for the undeformed ($w_0 = 0$) and normalized push down displacement $w_0^* = \frac{w_0}{R\tan\theta} = 0.75$ and 0.95. Fig. 2*D* shows linear dependence of the normalized contact radius $r_c^* = \frac{R_c}{R}$ on the push down displacement w_0^* in Eq. **3**.

The volume of the air trapped between the suction cup and rigid flat surface is

$$V = 2\pi\int_0^{R_c}[(R-r)\tan\theta - w]rdr. \qquad [4]$$

At the maximum push down displacement w_{0_max}, substitution of $w_{push\ down}$ in Eq. **2** into the above integral gives

$$V(w_{0\_max}) = \frac{4}{3}\pi\tan\theta\left(R - \frac{w_{0\_max}}{\tan\theta}\right)^3. \qquad [5]$$

Downloaded from https://www.pnas.org by NORTHWESTERN UNIVERSITY; SERIALS DEPARTMENT on July 2, 2026 from IP address 165.124.167.3.

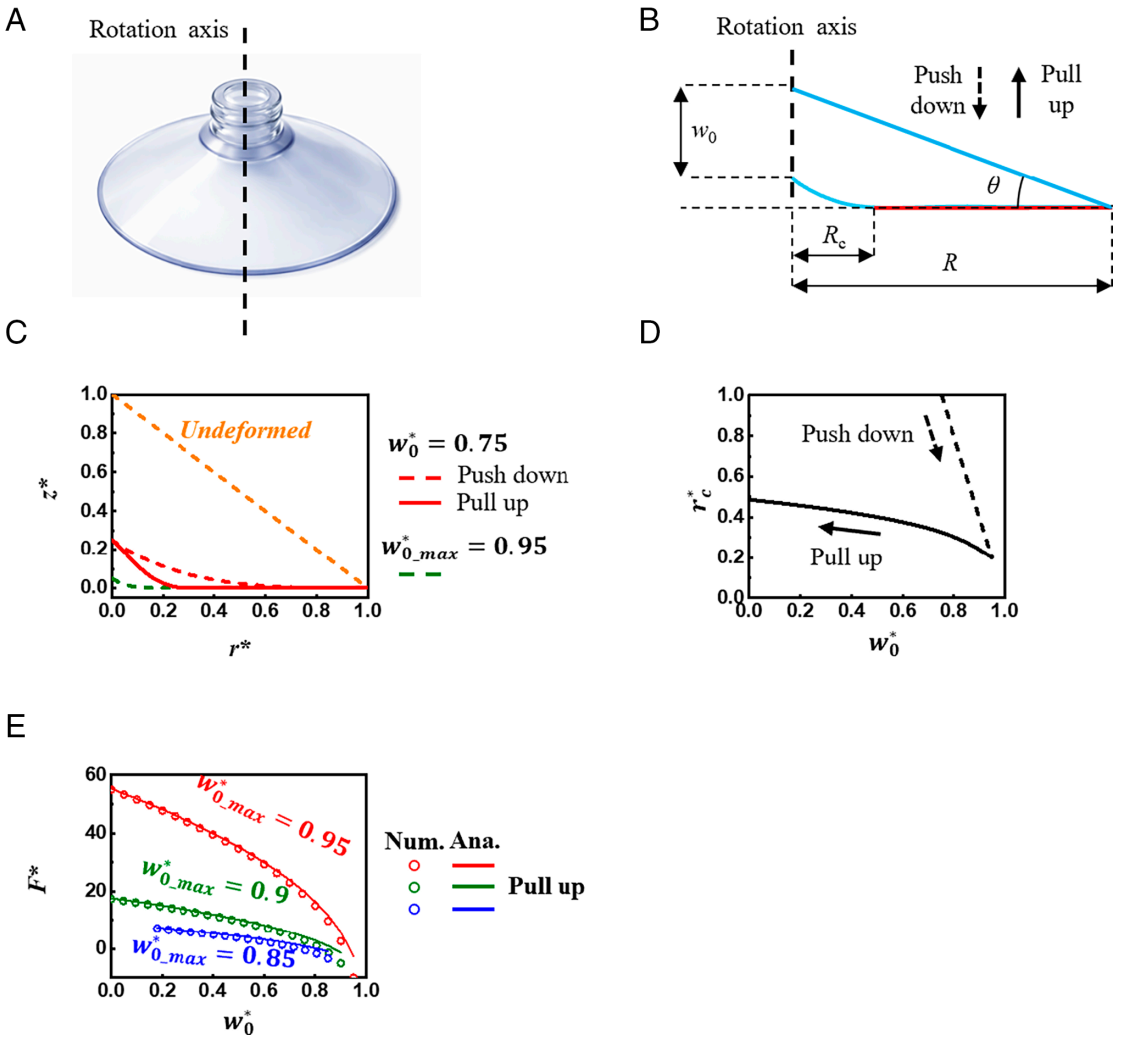

Fig. 2. Cone suction cup. (*A*) Schematic illustration of a cone suction cup, with (*B*) its axisymmetric geometry parameters at undeformed and deformed configurations. (*C*) The cross-sectional profile z^* during push down and pull up. (*D*) normalized contact radius r_c^* during push down and pull up. (*E*) Normalized pull up force F^* for both numerical (num.) and analytical (ana.) solutions.

After the deflection reaches its maximum w_{0_max} the suction cup is pulled up (Fig. 2*B*), i.e., w_0 decreases. The gas inside suction cup satisfies the ideal gas law $P_0 V(w_{0\_max}) = (P_0 - \Delta P) V(w_0)$ during pull up (25, 27), where P_0 is the atmosphere pressure inside the suction cup before pull up, $V(w_{0\_max})$ is given in Eq. **5**, $V(w_0)$ is the volume of suction cup during pull up obtained from Eq. **4** though its deflection w during pull up remains to be determined. The pressure drop ΔP inside the suction cup is then obtained as

$$\Delta P = \alpha P_0 \left[1 - \frac{V(w_{0\_max})}{V(w_0)}\right], \qquad [6]$$

where $\alpha = 1$ corresponds to the ideal gas law, which, however, could lead to a nonphysical decrease of the contact radius during pull up, as shown in *SI Appendix*, Fig. S1 and *Supplementary Note 2*. Therefore, α is introduced to ensure an increase of the contact radius during pull up. The maximum value of α is chosen thereby providing an upper-bound estimate of the maximum pull up force (*SI Appendix*, *Supplementary Note 2*).

For the noncontact region $(0, R_c)$ during pull up, the deflection is the sum of Eq. **2** (for push down) and the additional term due to the pressure difference ΔP,

$$w_{pull\ up} = w_{push\ down} + \frac{\Delta P}{64D} r^2 \left(r^2 - R_c^2 - 2R_c^2 \ln \frac{r}{R_c}\right). \qquad [7]$$

Its substitution into the integral in Eq. **4** gives $V(w_0)$, which together with modified ideal gas law in Eq. **6** and continuity condition of bending moment $w''(R_c) = 0$ across the interface, yield an algebraic equation for the contact radius R_c in *SI Appendix*, *Supplementary Note 2*. Fig. 2*C* also shows the profile ($z^* \sim r^*$) during pull up of the suction cup for the normalized maximum push down displacement $w_{0\_max}^* = \frac{w_{0\_max}}{R \tan\theta} = 0.95$. At the same displacement $w_0^* = 0.75$, the contact radius for pull up is much smaller than that for push down, reflecting the effect of gas law inside the suction cup. This is confirmed in Fig. 2*D* that the curve for pull up is much lower than push down.

Force equilibrium of the noncontact region of suction cup gives the pull up force $F_{pull\ up} = 2\pi R_c Q_r(R_c) + \pi R_c^2 \Delta P$, where $Q_r = -D\frac{d}{dr}\nabla^2 w_{pull\ up}$ is the shear force during pull up. The pull up force is obtained approximately in *SI Appendix*, *Supplementary Note 2* as

$$F_{pull\ up} \approx \frac{2\pi D \tan\theta}{R} \frac{1}{1 - w_0^*} \frac{1}{\lambda}\left(1 - \sqrt{\lambda}\right). \qquad [8]$$

Downloaded from https://www.pnas.org by NORTHWESTERN UNIVERSITY; SERIALS DEPARTMENT on July 2, 2026 from IP address 165.124.167.3.

For $\lambda = \sqrt{\frac{2\left(1-w^*_{0\_max}\right)^3}{\left(1-w^*_0\right)^3}} \ll 1$, which implies large push down ($w^*_{0\_max}$ close to 1) and moderate pull up ($w^*_0 < w^*_{0\_max}$). Further simplification by keeping only the lead term gives $F_{pull\ up} \approx \frac{2\pi D \tan\theta}{R}\sqrt{\frac{1-w^*_0}{2\left(1-w^*_{0\_max}\right)^3}}$ for $\sqrt{\lambda} = \sqrt[4]{\frac{2\left(1-w^*_{0\_max}\right)^3}{\left(1-w^*_0\right)^3}} \ll 1$. Fig. 2*E* shows that the normalized pull up force $F^* = \frac{RF_{pull\ up}}{2\pi D \tan\theta}$ vs. pull up displacement w^*_0 obtained from Eq. **8** agrees very well with the accurate (but numerical) solution (*SI Appendix, Supplementary Note 2*). The pull up force increases rapidly with the maximum push down displacement $w^*_{0\_max}$ = 0.85, 0.9, and 0.95, and it is orders of magnitude larger than the force during push down.

Ring Suction Cup. The ring suction cup, which is the representative geometry used for our recent skin-interfaced wearable device (illustrated in *SI Appendix*, Fig. S6) (22), is studied in order to further increase the pull up force. The schematic diagram in Fig. 3*A* shows the basic axisymmetric geometry of a ring suction cup placed on a rigid flat surface. Its axisymmetric cross-section (Fig. 3*B*) is an isosceles trapezoid with top radius R_1, bottom radius R_2, angle θ, and large rotation axis radius $\rho_0 \gg R_1, R_2$, in order to maximize the pull up force. Its top surface (radius R_1) attached to a rigid platform is pushed down by a uniform displacement w_0. The suction cup has nonadhesive surface contact after a relatively large w_0 and haws the same contact radius R_c on the outer and inner parts (Fig. 3*B*) to be determined. The analysis of outer (ρ_0+R_1, ρ_0+R_2) and inner (ρ_0-R_2, ρ_0-R_1) parts is essentially the same for $\rho_0 \gg R_1, R_2$ therefore only the outer part contact radius R_c is determined in the following.

For the outer contact region (ρ_0+R_c, ρ_0+R_2), the deflection is simply $w = (\rho_0+R_2-r)\tan\theta$, i.e., the vertical distance from the suction cup to the rigid flat surface at its bottom. This yields a vanishing second-order derivative $w'' = 0$ in the contact region. For the outer noncontact region (ρ_0+R_1, ρ_0+R_c), the pressure p in Eq. **1** is zero. The boundary conditions are $w(\rho_0+R_1) = w_0$ and zero slope $w'(\rho_0+R_1) = 0$, and continuity of deflection $w(\rho_0+R_c) = (R_2-R_c)\tan\theta$ and slope $w'(\rho_0+R_c) = -\tan\theta$ at the interface with the outer contact region. The deflection is then completely solved in *SI Appendix, Supplementary Note 3* as

$$w_{push\ down} = w_0 + 2\left[w_0 - \left(R_2 - \frac{R_1+R_c}{2}\right)\tan\theta\right]\left(\frac{x-R_1}{R_c-R_1}\right)^3 - 3\left[w_0 - \left(R_2 - \frac{R_1+2R_c}{3}\right)\tan\theta\right]\left(\frac{x-R_1}{R_c-R_1}\right)^2, \quad [9]$$

where $x = r - \rho_0$. Continuity condition of bending moment $w''(\rho_0+R_c) = 0$ across the interface yields the contact radius R_c during push down

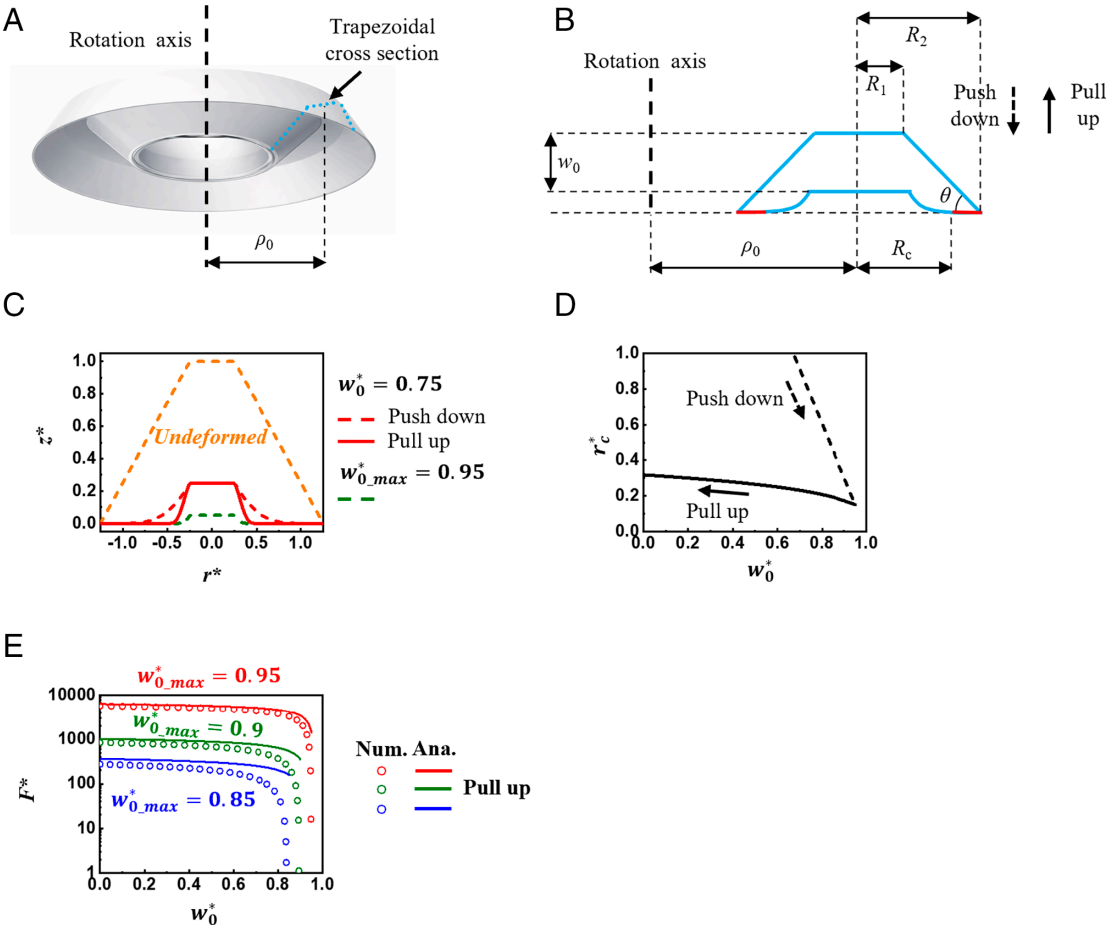

Fig. 3. Ring suction cup study. (*A*) Schematic illustration of a ring suction cup, with (*B*) its axisymmetric geometry parameters at undeformed and deformed configurations. (*C*) The cross-sectional profile z^* during push down and pull up. (*D*) normalized contact radius r^*_c during push down and pull up. (*E*) Normalized pull up force F^* for both numerical (num.) and analytical (ana.) solutions.

Downloaded from https://www.pnas.org by NORTHWESTERN UNIVERSITY; SERIALS DEPARTMENT on July 2, 2026 from IP address 165.124.167.3.

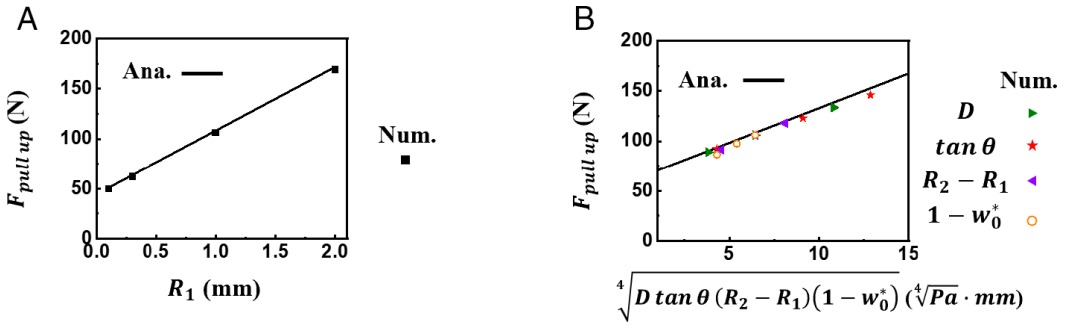

Fig. 4. The pull up force for ring suction cup vs. (*A*) R_1; (*B*) $\sqrt[4]{Dtan\theta(R_2-R_1)(1-w_0^*)}$.

$$R_c = 3R_2 - 2R_1 - 3\frac{w_0}{\tan\theta}. \quad [10]$$

The range of w_0 for surface contact should be $\left[\frac{2}{3}(R_2-R_1)\tan\theta, (R_2-R_1)\tan\theta\right]$. For $\frac{R_1}{R_2-R_1}=0.25$ (i.e., $\frac{R_1}{R_2}=0.8$) and $\rho_0^*=\frac{\rho_0}{R_2}=10$, Fig. 3*C* illustrates the normalized profiles ($z^*=\frac{(\rho_0+R_2-r)\tan\theta - w}{(R_2-R_1)\tan\theta}$ vs. $r^*=\frac{r-\rho_0}{R_2-R_1}$) during push down of the suction cup for the undeformed ($w_0^*=0$), and normalized push down displacement $w_0^*=\frac{w_0}{(R_2-R_1)\tan\theta}=0.75$ and 0.95 (FEA validation in *SI Appendix, Supplementary Note 5*). Fig. 3*D* shows linear dependence of the normalized contact radius $r_c^*=\frac{R_c-R_1}{R_2-R_1}$ on the push down displacement w_0^* in Eq. **10** for the outer and inner parts separately. At the maximum push down displacement w_{0_max}, the volume (for the initial trapezoid cross section) is

$$V(w_{0\_max}) = \pi\rho_0\tan\theta\left(R_2-R_1-\frac{w_{0\_max}}{\tan\theta}\right)\left(3R_2+R_1-3\frac{w_{0\_max}}{\tan\theta}\right). \quad [11]$$

Integration of deflection in Eq. **12** and $w(\rho_0-R_1<r<\rho_0+R_1)=w_0$ gives $V(w_0)$, which together with modified ideal gas law in Eq. **6** and continuity condition of bending moment $w''(\rho_0+R_c)=0$ across the interface, yield an algebraic equation for the contact radius R_c in *SI Appendix, Supplementary Note 4*. Fig. 3*C* also shows the profile (z^*~r^*) during pull up of the suction cup for the normalized maximum push down displacement $w_{0\_max}^*=\frac{w_{0\_max}}{(R_2-R_1)\tan\theta}=0.95$. At the same displacement $w_0^*=0.75$, the contact radius for pull up is much smaller than that for push down, reflecting the effect of gas law inside the suction cup. This is confirmed in Fig. 3*D* that the curve for pull up is much lower than push down.

Force equilibrium of the noncontact region of suction cup gives the pull up force $F_{pull\ up}=2\pi(\rho_0+R_c)Q_{r\_outer}(\rho_0+R_c)+2\pi(\rho_0-R_c)Q_{r\_inner}(\rho_0-R_c)+4\pi\rho_0R_c\Delta P$, where $Q_r=-D\frac{d}{dr}\nabla^2 w_{pull\ up}$ is the shear force during pull up. The pull up force is obtained approximately in *SI Appendix, Supplementary Note 4* as

$$F_{pull\ up}\approx\begin{cases}\dfrac{64\pi\rho_0 D\tan\theta}{9(R_2-R_1)^3(1-w_0^*)^3}\dfrac{1}{\lambda^2}\left[R_1\left(1-\sqrt[3]{\dfrac{\lambda^2}{2}}\right)+(R_2-R_1)\sqrt[4]{8}(1-w_0^*)\sqrt{\lambda}\right] \\ \qquad \text{for } 1-w_{0\_max}^* > \sqrt[3]{\dfrac{8D\tan\theta}{9P_0}}\dfrac{1}{R_2-R_1} \\ 4\pi\rho_0P_0\left[R_1\left(1-\sqrt[3]{\dfrac{\lambda^2}{2}}\right)+2\sqrt[4]{\dfrac{8D\tan\theta}{9P_0}(R_2-R_1)(1-w_0^*)}\right] \\ \qquad \text{for } 1-w_{0\_max}^* < \sqrt[3]{\dfrac{8D\tan\theta}{9P_0}}\dfrac{1}{R_2-R_1}\end{cases}. \quad [13]$$

After the deflection reaches its maximum w_{0_max} the suction cup is pulled up (Fig. 3*B*), i.e., w_0 decreases. The modified ideal gas law $\Delta P=\alpha P_0\left[1-\frac{V(w_{0\_max})}{V(w_0)}\right]$ in Eq. **6** holds, where α is determined in *SI Appendix, Supplementary Note 4*. For the outer noncontact region (ρ_0+R_1, ρ_0+R_c) during pull up, the deflection is the sum of Eq. **9** (for push down) and the additional term due to the pressure difference ΔP,

$$w_{pull\ up}=w_{push\ down}+\frac{\Delta P}{24D}(x-R_1)^2(x-R_c)^2. \quad [12]$$

for $\lambda=\sqrt{\frac{2\left(1-w_{0\_max}^*\right)^3}{\left(1-w_0^*\right)^3}}\ll 1$. For $\frac{R_1}{R_2-R_1}=0.25$ and $\rho_0^*=\frac{\rho_0}{R_2}=10$, Fig. 3*E* shows that the normalized pull up force $F^*=\frac{F_{pull\ up}}{2\pi\frac{\rho_0}{(R_2-R_1)^2}D\tan\theta}$ vs. pull up displacement w_0^* obtained from Eq. **13** agrees reasonably well with the accurate (but numerical) solution (*SI Appendix, Supplementary Note 4*). For the maximum push down displacement $w_{0\_max}^*$ = 0.85, 0.9, and 0.95, the pull up force increases and saturates rapidly as w_0 decreases, and it is

Downloaded from https://www.pnas.org by NORTHWESTERN UNIVERSITY; SERIALS DEPARTMENT on July 2, 2026 from IP address 165.124.167.3.

orders of magnitude larger than the force during push down. Compared with the cone suction cup, the ring geometry introduces additional design freedom through the rotation axis radius ρ_0 and the platform width R_1, enabling a much larger pull up force.

The pull up force increases monotonically with the maximum push down displacement w_{0_max}. At its limit $\boldsymbol{w}^*_{0\_max} \to 1$, the pull up force is

$$F_{pull\ up} \approx 4\pi\rho_0 P_0 \left[R_1 + 2\sqrt[4]{\frac{8D\tan\theta}{9P_0}\left(R_2 - R_1\right)\left(1 - w_0^*\right)}\right]. \quad [14]$$

which agrees very well with the accurate (but numerical) solution (*SI Appendix*, *Supplementary Note 4*) in Fig. 4 for the baseline values $D = 1.71 \times 10^{-6}$ N•m, $\rho_0 = 50$ mm, $\tan\theta = 0.25$, $R_1 = 1$ mm, $R_2 - R_1 = 4$ mm, $w^*_{0\_max} = 0.99$ and $w_0^* = 0$. Eq. **14** shows that the rotation axis radius ρ_0 increases the circumferential length of the suction interface, leading to linear scaling of the pull up force with ρ_0. The parameter R_1 controls the width of the flat platform and contributes to the effective area where the pressure difference acts such that the pull up force increases almost linearly with R_1 for fixed $R_2 - R_1$ (Fig. 4*A*). The wall width $R_2 - R_1$ determines the contact radius R_c through Eq. **10** and increases the force along with other parameters through a combination of $\sqrt[4]{D\ tan\ \theta\left(R_2 - R_1\right)\left(1 - w_0^*\right)}$ (Fig. 4*B*). These results indicate that enlarging ρ_0 and R_1 provides the most direct route to increasing the pull up force, whereas increasing $R_2 - R_1$ offers an additional but weaker contribution. A more general case with smaller $w^*_{0\_max}$ is discussed in *SI Appendix*, *Supplementary Note 4*. It should be pointed out that the above equation does not give the detachment force at which the suction cup detaches from the bottom surface as this force depends on the roughness, material, and small defects causing micro gas leakage channels (25, 30).

The present analytical model is validated by the finite element analysis for a deformable substrate (*SI Appendix*, Fig. S5 and *Supplementary Note 5*).

Conclusions

In summary, this work presents analytical models for the deformation and force of suction cups, spanning both the cone geometry and an optimized ring design, and thereby provides a systematic physical understanding of the push down and pull up processes. In contrast to previous studies, the analysis is carried out in a fully explicit form, without relying on indirect variables such as pressure difference ΔP and contact radius R_c that cannot be controlled/optimized. The formulae obtained agree well with the accurate numerical solutions, clearly reveal the roles of key geometric and material parameters in governing suction performance, and provide a quantitative foundation for the design and application of suction-based mounting strategies in wearable devices.

Materials and Methods

Finite Element Analysis. Finite element analysis was performed using the commercial software ABAQUS to examine the deformation of the ring suction cup during the push down process. The suction cup was modeled with axisymmetric shell elements (SAX1), with geometric nonlinearity enabled. Contact between the suction cup and the underlying substrate was modeled using hard normal contact and frictionless or penalty tangential contact. The substrate was modeled either as a rigid flat platform or as a deformable skin layer, depending on the simulation case. A prescribed vertical displacement was applied to the top surface of the suction cup. All materials were modeled as linear elastic. Mid-surface deformation profiles were extracted from the finite element results and compared with the analytical solutions. For strain analysis, strains at different shell section points, including the mid-surface and outer surfaces, were output.

Data, Materials, and Software Availability. All study data are included in the article and/or *SI Appendix*.

Author affiliations: [a]Department of Civil and Environmental Engineering, Northwestern University, Evanston, IL 60208; [b]Departments of Mechanical Engineering, Northwestern University, Evanston, IL 60208; [c]Querrey Simpson Institute for Bioelectronics, Northwestern University, Evanston, IL 60208; [d]Department of Materials Science and Engineering, Northwestern University, Evanston, IL 60208; [e]Department of Biomedical Engineering, Northwestern University, Evanston, IL 60208; and [f]Department of Neurological Surgery, Feinberg School of Medicine, Northwestern University, Chicago, IL 60611

1. J. A. Rogers, T. Someya, Y. G. Huang, Materials and mechanics for stretchable electronics. *Science* **327**, 1603–1607 (2010).
2. D. H. Kim *et al.*, Epidermal electronics. *Science* **333**, 838–843 (2011).
3. H. Jeong *et al.*, Differential cardiopulmonary monitoring system for artifact-canceled physiological tracking of athletes, workers, and COVID-19 patients. *Sci. Adv.* **7**, eabg3092 (2021).
4. J.-Y. Yoo *et al.*, Wireless broadband acousto-mechanical sensing system for continuous physiological monitoring. *Nat. Med.* **29**, 3137–3148 (2023).
5. J. T. Reeder *et al.*, Resettable skin interfaced microfluidic sweat collection devices with chemesthetic hydration feedback. *Nat. Commun.* **10**, 5513 (2019).
6. S. Cho *et al.*, Wearable lateral flow assays for cortisol monitoring with time-dynamic sweat sampling and sensing by electrochromic timers. *Nat. Sens.* **1**, 85–98 (2026).
7. C. Liu *et al.*, Wireless, skin-interfaced devices for pediatric critical care: Application to continuous, noninvasive blood pressure monitoring. *Adv. Healthc. Mater.* **10**, 2100383 (2021).
8. S. Li *et al.*, Measurement of blood pressure via a skin-mounted, non-invasive pressure sensor. *J. Appl. Mech.* **88**, 101008 (2021).
9. C. Nataraj, S. Hemmati, Harnessing nonlinear mechanics to transform medical diagnostics. *Appl. Mech. Rev.* **77**, 061001 (2025).
10. Z. Xie, D. Bai, J. Ma, C. Jing, M. Lu, Characterization of bilayer tissue moduli and thickness via eccentric rotating mass dynamics. *Appl. Mech. Rev.* **78**, 041001 (2026).
11. D. He, D. Malu, Y. Hu, A comprehensive review of indentation of gels and soft biological materials. *Appl. Mech. Rev.* **76**, 050802 (2024).
12. H. U. Chung *et al.*, Binodal, wireless epidermal electronic systems with in-sensor analytics for neonatal intensive care. *Science* **363**, eaau0780 (2019).
13. A. Y. Rwei *et al.*, A wireless, skin-interfaced biosensor for cerebral hemodynamic monitoring in pediatric care. *Proc. Natl. Acad. Sci. U.S.A.* **117**, 31674–31684 (2020).
14. L. Zhou, M. Guess, K. R. Kim, W. H. Yeo, Skin-interfacing wearable biosensors for smart health monitoring of infants and neonates. *Commun. Mater.* **5**, 72 (2024).
15. L. Fialho *et al.*, Exploring innovative adhesive approaches to manage medical adhesive-related skin injuries (MARSI). *Int. J. Adhes. Adhes.* **130**, 103636 (2024).
16. K. R. Jinkins *et al.*, Thermally switchable, crystallizable oil and silicone composite adhesives for skin-interfaced wearable devices. *Sci. Adv.* **8**, eabo0537 (2022).
17. T. Stuart *et al.*, Biosymbiotic, personalized, and digitally manufactured wireless devices for indefinite collection of high-fidelity biosignals. *Sci. Adv.* **7**, eabj3269 (2021).
18. S. Lee *et al.*, Deformation driven suction cups: A mechanics-based approach to wearable electronics. *Adv. Sci.* **13**, e20417 (2026).
19. M. K. Choi *et al.*, Cephalopod-inspired miniaturized suction cups for smart medical skin. *Adv. Healthc. Mater.* **5**, 80–87 (2016).
20. H. N. Mayrovitz, N. Sims, Effects of ankle-to-knee external pressures on skin blood perfusion under and distal to compression. *Adv. Skin Wound Care* **16**, 198–202 (2003).
21. F.-C. Huang, X.-D. Sun, Y. Shi, L.-J. Pan, Textile electronics for ubiquitous health monitoring. *Soft Sci.* **4**, 40 (2024).
22. J. Shin *et al.*, A non-contact wearable device for monitoring epidermal molecular flux. *Nature* **640**, 375–383 (2025).
23. J. Liu, K. Tanaka, L. Bao, I. Yamaura, Analytical modelling of suction cups used for window-cleaning robots. *Vacuum* **80**, 593–598 (2006).
24. D. Ge *et al.*, Quantitative study on the attachment and detachment of a passive suction cup. *Vacuum* **116**, 13–20 (2015).
25. A. Tiwari, B. N. J. Persson, Physics of suction cups. *Soft Matter* **15**, 9482–9499 (2019).
26. S. Song, D. M. Drotlef, D. Son, A. Koivikko, M. Sitti, Adaptive self-sealing suction-based soft robotic gripper. *Adv. Sci.* **8**, 2100641 (2021).
27. A. Bernardin *et al.*, Constraint-based simulation of passive suction cups. *ACM Trans. Graph.* **42**, 1–14 (2022).
28. L. Wang, K.-H. Ha, S. Qiao, N. Lu, Suction effects of crater arrays. *Extreme Mech. Lett.* **30**, 100496 (2019).
29. S. Timoshenko, S. Woinowsky-Krieger Theory of plates and shells (McGraw-Hill, ed. 2, 1959).
30. C.-Y. Li, X.-M. Liang, W.-K. Yuan, Y. Ding, G.-F. Wang, Size-dependent effects and surface roughness in contact mechanics. *Appl. Mech. Rev.* **78**, 010801 (2026).

Downloaded from https://www.pnas.org by NORTHWESTERN UNIVERSITY; SERIALS DEPARTMENT on July 2, 2026 from IP address 165.124.167.3.